

A PULSED, PRECESSING JET IN CEPHEUS A

NATHANIEL J. CUNNINGHAM¹, NICKOLAS MOECKEL^{2,3}, JOHN BALLY²

¹Department of Physics and Astronomy, University of Nebraska-Lincoln, 116 Brace Laboratory, Lincoln, NE 68588-0111

²Center for Astrophysics and Space Astronomy, University of Colorado, 389 UCB, Boulder, CO 80309-0389 and

³School of Physics & Astronomy, University of St Andrews, St Andrews KY16 9SS, Scotland

Draft version November 6, 2018

ABSTRACT

We present near-infrared H₂, radio CO, and thermal infrared observations of the nearby massive star-forming region Cepheus A (Cep A). From H₂ bow shocks arranged along four distinct jet axes, we infer that the massive protostellar source HW2 drives a pulsed, precessing jet that has changed its orientation by about 45° in roughly 10⁴ years. The current HW2 radio jet represents the most recent event in this time series of eruptions. This scenario is consistent with the recent discovery of a disk around HW2, perpendicular to the current jet orientation, and with the presence of companions at projected distances comparable to the disk radius. We propose that the Cep A system formed by the disk-assisted capture of a sibling star by HW2. We present a numerical model of a 15 M_⊙ star with a circumstellar disk, orbited by a companion in an inclined, eccentric orbit. Close passages of the companion through or near the disk result in periods of enhanced accretion and mass loss, as well as forced precession of the disk and associated orientation changes in the jet. The observations reveal a second powerful outflow that emerges from radio source HW3c or HW3d. This flow is associated with blueshifted CO emission and a faint H₂ bow shock to the east, and with HH 168 to the west. A collision between the flows from HW2 and HW3c/d may be responsible for X-ray and radio continuum emission in Cep A West.

Subject headings: ISM: jets and outflows — ISM: Herbig-Haro objects — ISM: kinematics and dynamics — ISM: individual: CepA — stars: formation

1. INTRODUCTION

Collimated, bipolar outflows accompany the birth of young stars from the earliest stages of star formation to the end of their accretion phase (e.g. Reipurth & Bally 2001; Bally et al. 2006). The structure and kinematics of these flows provide a fossil record of the mass-loss histories of the associated young stellar objects (YSOs); the most distant shocks trace the oldest major mass-loss events while inner jets and shocks provide clues about the recent processes. The structure and symmetries of outflows record orientation changes of the underlying accretion disk and motion of the outflow sources relative to the surrounding interstellar medium (ISM). For example, C-shaped outflows may indicate deflection by a side-wind (e.g., within expanding plasma of the Orion Nebula, Bally et al. 2006); other C-shaped bends may result from motion of the source YSO through the medium, possibly ejected by dynamical processes in a young cluster (e.g., HH 498 in NGC 1333, Bally & Reipurth 2001; HH 366 in Barnard 5, Yu et al. 1999). Point-symmetric S- or Z-shaped bends can be produced by the precession of a circumstellar disk. Examples of this kind of symmetry include HH 199 in the L1228 cloud (Bally et al. 1995) and 20126+4104 (Su et al. 2007). Such outflow orientation changes may provide indirect evidence for a companion star in an orbit inclined relative to the disk, inducing forced precession.

In this paper, we present images of shocked outflows in the Cep A star-forming region, together with radial velocity maps of CO emission. We interpret the outflow morphology as evidence that the massive protostar HW2 drives a pulsed, precessing jet whose orientation changes may be induced by the periastron passage of a moderate-mass companion in an ec-

centric, non-coplanar orbit. We present a numerical model that demonstrates the plausibility of jet precession forced by a companion for the case of HW2.

1.1. Overview of Cep A

The Cep A star-forming complex contains the second nearest region of massive star formation, after the Orion complex. Located at a distance of 725 pc (Blaauw et al. 1959; Crawford & Barnes 1970), the Cepheus OB3 association contains a 20 by 60 pc molecular cloud that houses six localized peaks of CO emission, designated Cep A through F (Sargent 1977, 1979). Cep A contains dense molecular clumps (Torrelles et al. 1993), molecular outflows (Rodríguez et al. 1980a; Narayanan & Walker 1996; Gómez et al. 1999), H₂O and OH masers (Cohen et al. 1984), hyper-compact H II regions (Hughes & Wouterloot 1984), variable radio continuum sources (Garay et al. 1996), Herbig-Haro objects (Hartigan et al. 1986), bright shock-excited H₂ emission (Hartigan et al. 2000), a cluster of far-infrared (FIR) sources with a luminosity of 2.5 × 10⁴ L_⊙ (Koppenaal et al. 1979), and a cluster of Class I and Class II YSOs (Gutermuth et al. 2005). The bulk of the region's luminosity likely arises from radio sources HW2 and HW3c/d (Hughes & Wouterloot 1984) that are associated with bright H₂O masers.

Cep A contains a massive bipolar molecular outflow aligned primarily east-west (Rodríguez et al. 1980b), but with additional components aligned northeast-southwest (Bally & Lane 1990; Torrelles et al. 1993; Narayanan & Walker 1996; Gómez et al. 1999). The central 2' region contains high velocity (HV) as well as more compact extremely high velocity (EHV) CO components with radial velocities ranging from -50 to 70 km s⁻¹ relative to the CO centroid (Narayanan & Walker 1996). The axis of the EHV outflow is rotated roughly 40° clockwise relative

Electronic address: ncunningham2@unl.edu
Electronic address: Nickolas.MoECKel@colorado.edu
Electronic address: John.Bally@colorado.edu

to the HV outflow on the plane of the sky. The smaller spatial extent together with the higher velocity suggests that the EHV flow traces a younger outflow component. Several self-absorption dips follow trends seen in the low-velocity line wings, with regions east of HW2 blueshifted and west of HW2 redshifted. Thus cooler, self-absorbing gas traces the low-velocity bipolar outflow rather than the quasi-stationary ambient medium. At low velocities, there are additional blue- and redshifted components centered on HW2 that are oriented northeast–southwest.

The Cep A outflow complex contains several Herbig–Haro objects, including the extremely bright HH 168 located about $90''$ due west of HW2, and several fainter bow shocks located to the east (Hartigan et al. 2000). Fainter HH objects (HH 169 and 174) are located in the eastern, blueshifted lobe. Near-infrared (NIR) images show an extremely bright reflection nebula centered on HW2 with an illumination cone that opens toward the northeast. The $2.12 \mu\text{m}$ H_2 line exhibits a complex, filamentary structure.

There are multiple luminous sources in the complex of HW radio sources at the core of the Cep A region, led by HW2, and including HW3c, HW3d, and perhaps HW3a, HW8, and HW9. To the west, it has been proposed that radio source W-2 may also be internally heated. Because some of these (HW2, HW3d, W-2) have the radio signatures of jets, these are likely candidates for driving the outflows observed in CO and other molecules as well as the shocks traced by H_2 , Fe II, and optical HH emission. The complexity of the outflows, their multiple orientations, ages, and velocities, and the unclear morphology of some of the shock features make Cep A challenging to interpret. Are deflections involved, as suggested by Goetz et al. (1998)? Are there additional outflow sources we have not yet detected? Are we confusing externally shocked or jet-heated features with self-luminous sources?

HW2 is the strongest radio continuum source in the region with a flux density of $15.8 \pm 0.3 \text{ mJy}$ at 14.9 GHz (Garay et al. 1996); it may be the most luminous source in Cep A with $L \approx 10^4 L_\odot$, implying a mass of 15–20 M_\odot . HW2 is located near the center of a small ($< 5''$), dense clump apparent in the NH_3 maps of Torrelles et al. (1993) at the tip of one of the larger NH_3 concentrations. Multi-frequency observations by Rodríguez et al. (1994) using the VLA show that HW2 is elongated, and that both its spectral index and size versus frequency relation match those expected for a biconical thermal jet. Higher angular resolution observations (Hughes et al. 1995; Hoare & Garrington 1995) show that HW2 contains a clumpy radio continuum jet whose knots have proper motions of order 500 km s^{-1} (Curiel et al. 2006). Many models of the region postulate that HW2 is the major or sole source of outflows in the region.

The recent interferometric observations of the dust continuum, free–free emission, and several molecular tracers with arcsecond and subarcsecond angular resolution have shown that HW2 is surrounded by a complex dust distribution and several close-by protostars. A hot core that must contain a moderate-mass YSO is located about 400 AU east of HW2 (Martín-Pintado et al. 2005). VLA observations reveal a supposedly low-mass protostar that emits radio waves and is located at the center of the H_2O maser arc detected by Torrelles et al. (2001b). HW2 is surrounded by a circumstellar disk at least several hundred AU in radius and likely by several low-mass protostars (Rodríguez et al. 2005; Patel et al. 2005; Brogan et al. 2007; Comito et al. 2007;

Table 1
NIC-FPS OBSERVATIONS OF CEPHEUS A

Date	Filter	Number of exposures	Exposure time (s)	
			each	total
2005 Dec 11	H_2 - $2.12 \mu\text{m}$	10	240	2400
	K_s	5	20	100
2006 Jan 12	H_2 - $2.12 \mu\text{m}$	5	240	1200
	K_s	20	12	240
2007 Jan 29	J	15	20	300
	H	15	20	300
	K_s	15	20	300

Jiménez-Serra et al. 2007; Torrelles et al. 2007).

The radio sources Cep A HW3d and HW3b are also associated with a clusters of H_2O masers. HW3c and/or HW3d are suspected to be moderate-mass protostars. They are located $5''$ south of HW2 and close to the western end of a nearly continuous chain of radio sources along the southern rim of the Cep A East radio source complex. The eastern part of this chain may in part trace a radio continuum jet from HW3c/d at about P.A. $\approx 100^\circ$. The counter-jet direction points directly at the radio source W-2 at the eastern end of HH 168 in Cep A West.

Submillimeter wavelength continuum interferometry at $875 \mu\text{m}$ (Brogan et al. 2007) shows strong dust emission from HW2, HW3c, and extended emission to the southwest near HW3a. No submm continuum was detected from HW3d, leading these authors to conclude that HW3c is most likely to harbor the second most luminous and massive YSO in the Cep A core. In this interpretation, radio source 3d may trace part of a thermal jet from HW3c. The associated maser emission may be an indicator of shocks in a dense molecular gas. For the rest of this paper, we will assume that the dominant energy source is embedded in HW3c, but our interpretation does not depend critically on which peak, HW3c or 3d, contains the source.

The extinction to the HW sources is extremely large with $A_V \approx 500$ to 1000 magnitudes. Thus, none of these radio continuum sources is visible in the NIR. An extremely bright infrared (IR) reflection nebula emerges from the vicinity of HW2 toward P.A. $\approx 60^\circ$. The IR continuum polarization vectors indicate that the illumination is coming from the direction of HW2, HW3, and HW8 (Colome & Harvey 1995). However, the accuracy of polarization measurements is insufficient to determine the source unequivocally.

2. OBSERVATIONS

2.1. NIR Imaging

We observed Cep A on three nights from 2005 to 2007, using the Near Infrared Camera/Fabry Perot Spectrograph (NIC-FPS) on the Astrophysical Research Consortium 3.5m telescope at Apache Point Observatory, New Mexico. The NIR emission in the Cep A region spans $9'$ east to west, and requires at least two telescope pointings for complete coverage with the $4.6' \times 4.6'$ field-of-view of NIC-FPS. On each occasion, the total exposure time was evenly split between a western field and an eastern field. We obtained broadband images in J, H, and K_s filters of the Mauna Kea filter set, and in a narrowband (0.4% bandpass) filter centered on the H_2 $2.12 \mu\text{m}$ line. The dates and details of observations taken on each night are listed in Table 1.

Images were taken in dithered sets of 5 or 15 frames; individual frames were reduced by performing dark and sky sub-

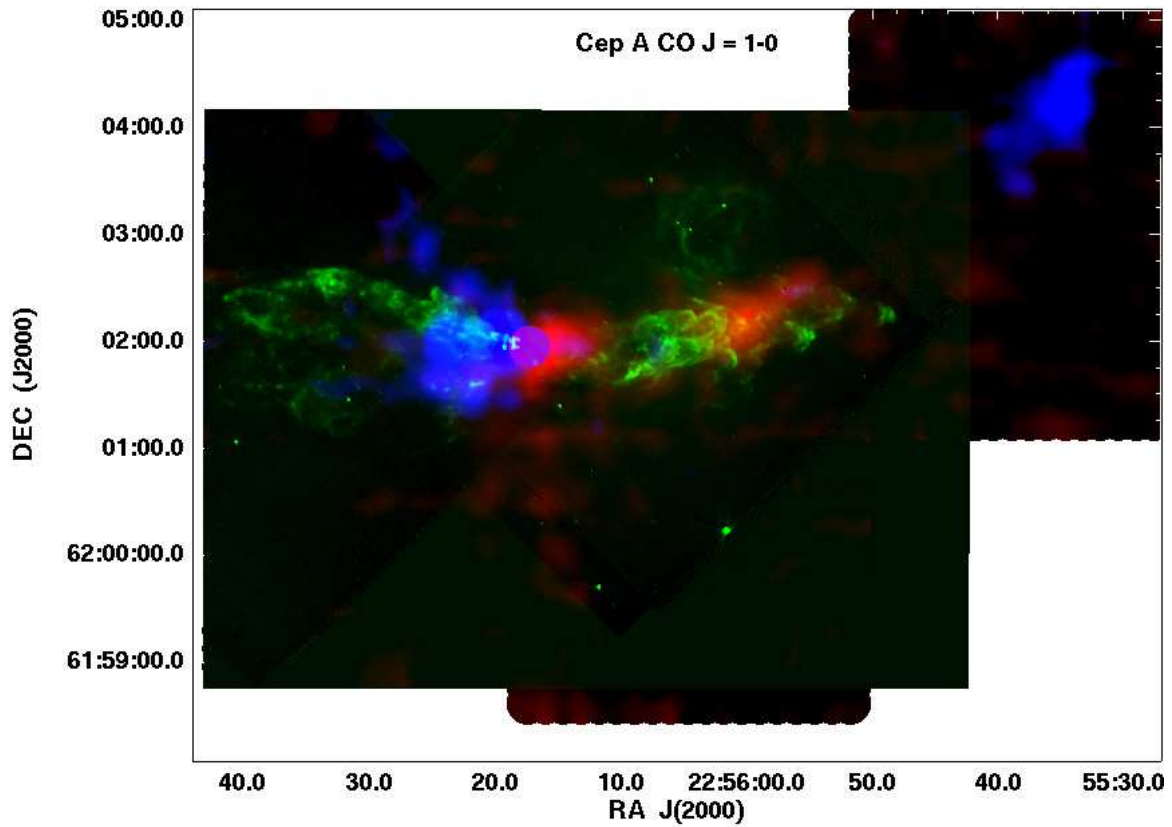


Figure 1. The $2.12\ \mu\text{m}$ H_2 emission (green) superimposed on emission from high-velocity CO with $-27 < V_{\text{LSR}} < -18\ \text{km s}^{-1}$ (blue) and $-3 < V_{\text{LSR}} < 6\ \text{km s}^{-1}$ (red). In this (and the next two figures) the purple circle shows a beam-sized spot at the location of HW2.

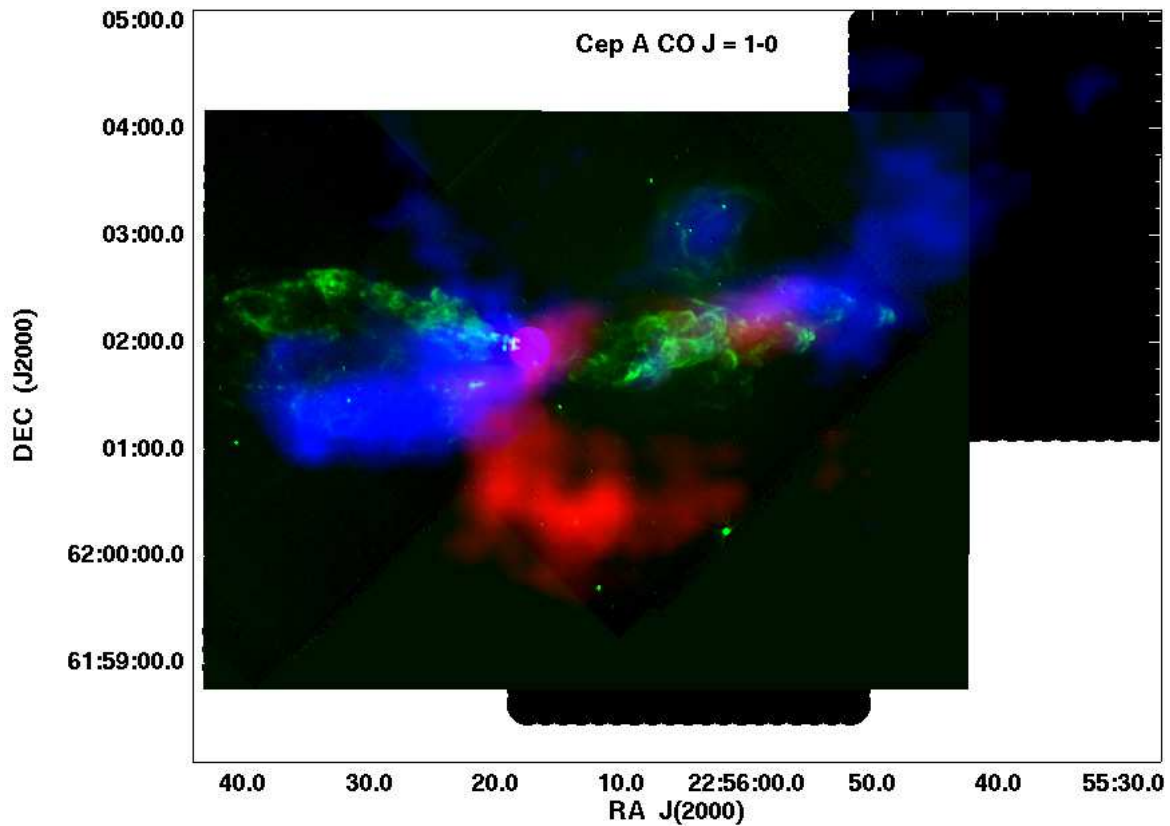


Figure 2. The $2.12\ \mu\text{m}$ H_2 emission (green), and emission from moderate-velocity CO with $-18 < V_{\text{LSR}} < -13\ \text{km s}^{-1}$ (blue) and $-6 < V_{\text{LSR}} < -3\ \text{km s}^{-1}$ (red).

traction, flat fielding, and correction for instrumental geometric distortion. Frames in each set were then co-aligned and median combined to eliminate bad pixels and to reduce noise. Registration to absolute coordinates was achieved by matching locations of many point sources in each combined image to stellar J2000 coordinates for the region from the 2MASS project. Once properly registered to this common frame, all the images taken in a single filter were co-added; each region of the combined image was scaled to properly account for a varying number of overlapping images and differing exposure times.

As the H_2 2.12 μm narrowband filter falls within the bandpass of the K_s filter, the latter was used as a proxy for the continuum that contaminates the H_2 emission in the narrowband image. We removed the continuum component by subtracting a scaled version of the final K_s image from the same nights as the H_2 observations. The scale factor was chosen based on the best continuum removal as judged by eye in the subtracted image. Variations in seeing between the narrowband and broadband exposures result in the incomplete removal of some stars.

2.2. Optical spectroscopy

Visual wavelength long-slit spectra of the shocks located east and northeast of Cep A HW2 were obtained with the Double Imaging Spectrograph (DIS) at the f/10 Nasmyth focus of the 3.5 meter reflector at the Apache Point Observatory on 2007 January 9. A 1.5'' wide by 5' long slit was used with a grating providing a spectral resolution $R = \lambda/\Delta\lambda \approx 5,000$. At each slit orientation three images with exposure times of 10 minutes were obtained.

2.3. Radio observations

The Nobeyama Radio Observatory (NRO) 45 m radio telescope was used in February 1987 to map the distribution of $\text{J}=1-0$ ^{12}CO from the Cep A outflow complex with 15'' resolution at 115 GHz. Nobeyama spectra were collected on a uniform grid with a 10'' spacing over a 5 by 9 arcmin region containing the Cep A outflow complex. Over 1900 individual positions were observed for an average integration time of about 1 min per position, with 20 seconds on source and 20 seconds off source plus 10 seconds of dead time used for reading the spectrometer, and moving the antenna after each 20 second integration period. Approximately 14 separate 10-hr periods were devoted to observing Cep A. A cooled Schottky receiver with a single sideband receiver temperature $T_{SSB} \approx 350\text{K}$ was used in conjunction with both a high (25 kHz/channel) and a low resolution (100 kHz/channel) 2048 channel acousto-optic spectrometer (AOS). All data were calibrated using the standard chopper wheel method. Pointing was monitored every 2 hr by observations of 43 GHz SiO maser emission from nearby late-type giant stars using a separate receiver system. Both high- and low-resolution AOSs were used to record spectra. The noise temperature of this receiver fluctuated between $T_{SSB} \approx 800\text{K}$ and infinity due to a problem, so data in these lines are available only over parts of the source. Spectra were obtained by position-switching to an emission-free reference position about 20' to the northwest. The data were reduced using the COMB package developed by R. W. Wilson at AT&T Bell Laboratories.

2.4. Thermal IR Imaging

Observations of the Cep A region were made using the Keck Observatory facility mid-IR camera Long Wave Spectrometer (LWS) on 2002 November 16. LWS is a mid-IR imaging and spectroscopy instrument mounted on the forward Cassegrain focus of Keck I, employing a Boeing 128×128 As:Si BIB array with a $10.2'' \times 10.2''$ field of view (Jones & Puetter 1993). Weather conditions were poor; the thermal background and atmospheric transmission varied by 50% throughout the first half of the night. Approximately 10 individual observations (frames) were obtained at slightly overlapping positions using the 12.5 μm filter (12 to 13 μm bandpass with $> 80\%$ transmission). The chopping secondary mirror was driven at 2 Hz with a 30'' east–west throw. Each frame was observed using the standard mid-IR chop-nod technique with two chopping positions plus (on-source) and minus (off-source); after chopping with the source in chop-beam plus, the telescope was nodded along the chop axis so that the object would sit in chop-beam minus, and chopping would continue. Each frame was observed for one complete chop-nod cycle, yielding a total on-source integration time of 27.6 s per mosaic frame. The standard stars β Peg, β And, and β Gem were observed for point-spread function (PSF) determination and flux calibration. The images are nearly diffraction limited at 12.5 μm with PSF FWHM = 0.38'' and a Strehl ratio of 35%. Data reduction details are given in Shuping et al. (2004). The image coordinates are accurate to about 1''.

2.5. Observational results and interpretation

2.5.1. The CO Outflow Complex

NRO single-dish observations of accelerated CO emission provide constraints on the past evolution of the Cep A outflow complex. While radio jets and HH objects near their sources tend to trace the highest velocity and recently ejected outflow components with velocities higher than a few hundred km s^{-1} , HH objects located far from their sources and shock-excited H_2 emission tend to trace moderate speeds of 10 to about 200 km s^{-1} . CO and other molecules trace the gas swept up by secondary interactions with the ambient medium and have velocities of a few to tens of km s^{-1} . Thus, CO and similar tracers tend to act as calorimeters of the total amount of momentum injected into the parent cloud by the faster flow components.

The NRO CO data (Figures 1, 2, and 3) show a prominent outflow complex with complicated structure. In general, the Cep A CO emission is collimated along an east–west direction at the highest velocities, while at the lowest velocities, the CO emission is very poorly collimated and bipolar along a northeast–southwest direction. At velocities more than about 8 km s^{-1} away from the rest velocity of the Cep A core (-11 km s^{-1} relative to the local standard of rest), the strongest outflow component consists of an east–west bipolar flow that is blueshifted toward the east (blue component in Figure 1) and redshifted toward the west. Additionally, an anomalous blueshifted lobe appears about 6' west by northwest of HW2 (upper-right corner of Figure 1). A fainter bipolar component, blueshifted toward the northeast and redshifted toward the southwest, emerges from the HW2 region at P.A. $\approx 35^\circ$; this is most apparent at moderate velocities (diagonal bipolar feature in Figure 2). At low velocities of about 2–5 km s^{-1} with respect to the centroid velocity, a prominent blueshifted lobe emerges from near HW3c (located about 5'' south of HW2) and extends about 2' east at P.A. $\approx 100^\circ$. Below, it is argued that this feature traces an outflow from HW3c.

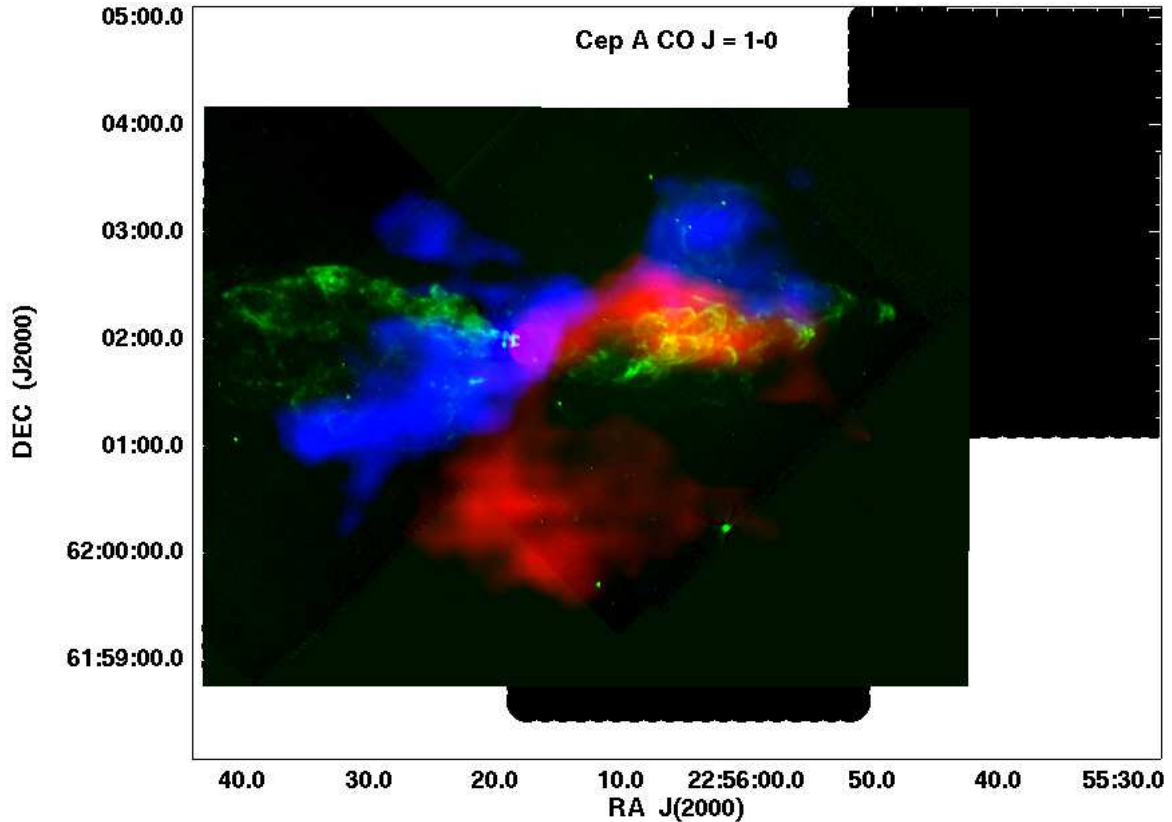


Figure 3. The $2.12 \mu\text{m}$ H_2 emission (green), and emission from low-velocity CO with $-15 < V_{\text{LSR}} < -13 \text{ km s}^{-1}$ (blue) and $-8 < V_{\text{LSR}} < -6 \text{ km s}^{-1}$ (red).

Rather than tracing two independent flows, the brighter east–west outflow from HW2 and the secondary, weaker outflow component oriented northeast–southwest at P.A. $\approx 35^\circ$ may trace the walls of a large-scale bipolar cavity that opens toward the northeast and southwest. In this interpretation, the northeast cavity walls are at P.A. $\approx 100^\circ$ and 40° and the southwest cavity walls are at P.A. $\approx 280^\circ$ and 200° . The orientation of the IR reflection nebula emerging from the HW2 region (Figure 5) provides support for this scenario; its axis lies at P.A. $\approx 70^\circ$, which is aligned with the opening of the northeast cavity.

2.5.2. The Core in the Mid-IR

Figure 4 shows the Keck $12.5 \mu\text{m}$ image of the Cep A core. The brightest feature is the double-lobed nebulosity surrounding the position of HW2. The two peaks of mid-IR emission are separated by about $1.4''$ along an axis oriented at P.A. $= 45^\circ$, which is similar to the orientation of the HW2 radio continuum jet. The dark lane that separates the two emission peaks has an orientation similar to the circumstellar disk surrounding HW2. However, it is unclear whether the dark lane is an IR disk shadow produced by a more compact disk surrounding HW2, or the gap is actually the disk seen in silhouette. Multicolor imaging is needed to determine the nature of the gap. No prominent mid-IR sources are seen at the locations of radio sources HW3c and d. However, an extended IR nebula is visible about $2''$ west of HW3c. This feature might be illuminated by either HW2, 3c, or 3d. IR polarization measurements are needed to distinguish these possibilities.

A faint point source is located at J(2000) = 22:56:18.2, +62:01:44. Although there are no NIR sources at this location, there is an H_2O maser spot ($\text{H}_2\text{O-E}$) located $0.7''$ from

the nominal mid-IR source position.

2.5.3. Radial Velocities of Optical HH Objects

In contrast to the spectacular 300 km s^{-1} Doppler shifts seen toward HH 168 in Cep A West, the long-slit spectra of the faint HH objects HH 169 and 174 located east and northeast of HW2 show only small Doppler shifts not larger than about 60 km s^{-1} in the core of the line profile. All components to the east are blueshifted. The radio proper motions of the continuum jet emerging from HW2 indicate velocities of order 500 to 300 km s^{-1} within a few seconds of the source. Thus, it may seem surprising that shocks located at distances of 1 – $5'$ away show much lower velocities. The low velocities either indicate that the flow east of HW2 is mostly along the plane of the sky, or that the ejecta have been decelerated significantly. Future proper motion measurements are needed to distinguish these possibilities. However, most HH objects exhibit rapid decreases in their velocities with increasing distance from their sources (Reipurth & Bally 2001; Devine et al. 1997). Such deceleration is probably caused by the interaction of the ejecta with the ambient medium. The structure of the Cep A cloud is such that the outflows emerging from the Cep A core propagate relatively freely toward the west, but impact dense molecular gas toward the east. Thus, it is not surprising that HH 168 has high velocities while the eastern shocks associated with HH 169 and 174 have low velocities. For the rest of the paper, we assume that the space velocities of the ejecta east of the Cep A core have a speed of about 100 km s^{-1} , typical of HH objects located at comparable distance from their sources.

2.5.4. The H_2 Outflow Complex

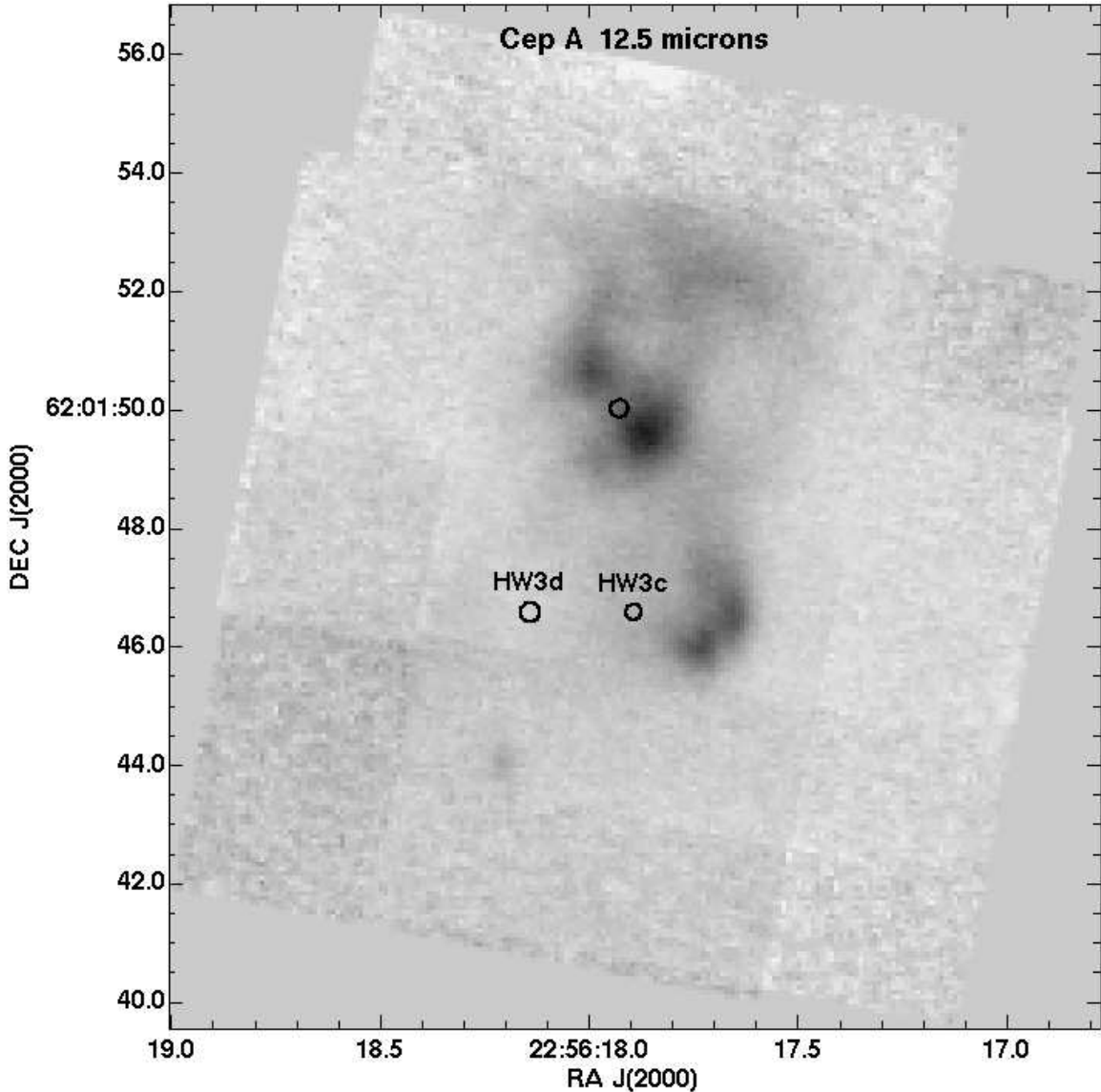


Figure 4. The Cep A core at $12.5 \mu\text{m}$ observed with LWS on the Keck 10 m telescope. The locations of the three suspected most massive protostars are shown in black circles. HW2 is the unlabeled circle.

Figure 5 shows a three-color composite image built from the J, H, and K_s broadband filter images. The continuum-subtracted narrowband image of the H_2 emission in the Cep A complex is displayed in Figure 6, and is shown in relation to the CO emission in Figures 1–3. The narrowband image exhibits three main components: shock emission east of the central protostellar cores containing HW2 and HW3c/d, bright arcs of shock-excited emission located to the west of these cores that is associated with HH 168, and a faint rosette of emission to the northwest. The rosette is associated with an east-facing globule or small pillar, located about $1.5'$ north of HH 168, which exhibits slightly blueshifted CO emission in Figures 2 and 3. The H_2 emission is likely to be excited by UV radiation from the Cep OB3 association and is thus probably fluorescent in nature. The globule contains an $m_B = 16$ magnitude star that is also called Cep A IRS2. Because there is no redshifted emission in this region, the blueshifted CO emission is unlikely to be a tracer of an outflow. The CO velocity field in the globule may reflect random motions within the Cep A cloud, or be the result of UV-photo-heating-induced

ablation of the globule surface that can accelerate gas to a velocity of a few km s^{-1} .

2.5.5. Bipolar Outflow from HW3c: HH 168 and its Counterflow

The series of bright arcs and H_2 bow shocks located $1\text{--}3'$ west of HW2 are associated with HH 168. The axes of symmetry of most of these shocks indicate a point of origin about $10''$ south of HW2. The submillimeter and radio continuum source HW3c and the bright H_2O maser and radio source HW3d lie on or near this axis. A dim, $40''$ diameter bow shock is located on this axis about $2'$ east of HW3c, directly opposite HH 168. This feature and the visual-wavelength part of HH 168 are symmetrically placed about HW3c. Thus, HW3c is likely to be the source of these shocks and the associated CO outflow components. High-resolution cm-wavelength VLA observations (Garay et al. 1996) reveal a chain of radio sources approximately aligned with the axis of this flow; these may either trace an ionized jet, or the interface between a jet and surrounding dense cloud material.

Figures 2 and 3 show that the bipolar outflow from HW3c



Figure 5. Color-combined broadband image of Cep A. J-band emission is shown in blue, H in green, and K_s in red.

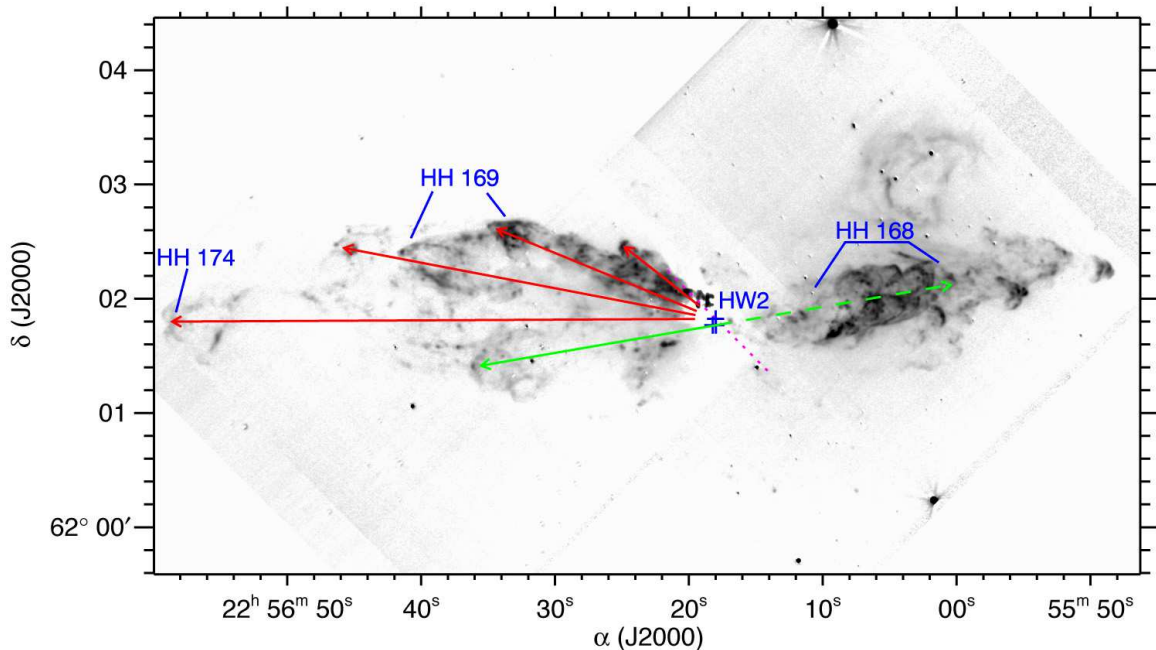


Figure 6. Continuum-subtracted $2.12 \mu\text{m}$ H_2 emission in the Cep A outflow complex. The successive orientations of a suspected precessing jet from HW2 are indicated by red arrows; the position of HW2 is marked with a cross. The oldest (eastward) ejection appears to power HH 174 to the east. The next two ejections may be responsible for HH 169. The current orientation of the radio jet emerging from HW2 is at position angle (P.A.) = 45° , indicated by the dashed magenta line. Bright HH 168, and the H_2 bows at far right, may result from an outflow from HW3c or HW3d (also marked with crosses) along the green axis. A faint H_2 bow marks the opposite lobe of this flow.

is associated with low-velocity to intermediate-velocity red- and blueshifted gas. The bright jet-like H_2 feature located $30''$ east of HW3c is associated with the strongest blueshifted CO emission. However, about $1'$ east, the blueshifted CO lobe shifts about $15''$ south of the flow axis and terminates just below (south) of the H_2 bow shock. Evidently, the HW3c flow interacts strongly with ambient cloud material along its south wall. However, there appears to be less interaction along the north rim of this cavity, perhaps because ambient material in this region has been cleared away by the HW2 flow.

The western lobe of this flow is associated with redshifted CO co-located with HH 168. Three bow shocks bright in H_2

lie on the southern side of HH 168; their orientations are consistent with a flow powered by HW3c. The bow shock morphologies and low CO velocities indicate that this flow lies close to the plane of the sky. It is somewhat unusual that at visual and NIR wavelengths, the redshifted outflow lobe is brighter than the blueshifted lobe. This feature may be a consequence of the morphology of the Cep A cloud core that appears to be mostly located east of the region containing HW2 and HW3c. The large range of radial velocities observed in HH 168 in visual-wavelength spectra may indicate sideways splashing of the high velocity ejecta moving mostly in the plane of the sky that has encountered slower-moving mate-

rial.

2.5.6. Non-detection of Source W-2 in HH 168 in the IR

Radio source W is located at the eastern end of the HH 168 shock complex in Cep A West. The radio emission from this object is extended with an elongation similar to that of the shocked H₂ emission. Based on radio spectral indices, Garay et al. (1996) infer that subcomponent W-2 houses an ultracompact internal source, shielded from view in the IR by the surrounding molecular cloud, and that the elongated radio emission is likely due to a jet launched by this source. Our images exhibit co-located, intense NIR H₂ emission that coincides with bright optical HH features at the eastern end of HH 168, making it unlikely that this region is highly obscured. Yet the broadband NIR images do not reveal any point sources in this region; thus it seems unlikely that a stellar source exists at this location. Rather, radio source W may trace a hard shock, with speeds above 400 km s⁻¹. The detection of soft X-ray emission from this region (Pravdo & Tsuboi 2005) provides support for this interpretation. Source W is located where two outflows, one emerging from HW2 and another from HW3c, intersect on the plane of the sky. Thus it is possible that these flows are actually colliding. We suggest that the radio and X-ray emission from HW may arise from colliding flows emerging from the two most massive protostars in Cep A East. This interpretation is generally in line with the westward proper motions measured for this radio source (Rodríguez et al. 2005).

2.5.7. A Pulsed, Precessing Outflow from HW2

The blueshifted, eastern lobe of the Cep A outflow contains four distinct chains of H₂ emitting features, each of which terminates in a well-formed bow shock. The four chains appear to emerge from the immediate vicinity of HW2. Their axes, defined by lines connecting HW2 to the bow shocks at the eastern and north-eastern ends of the chains, shift systematically clockwise from nearly east–west to northeast–southwest. The longest chain, which terminates 4.8' East of HW2 at HH 174, has a position angle P.A. $\approx 90^\circ$. The second chain, which terminates about 3.4' from HW2 at the eastern component of HH 169, has P.A. $\approx 80^\circ$. The third chain terminates at the western component of HH 169, about 2.2' northeast of HW2 and has P.A. $\approx 65^\circ$. The fourth chain ends in a bright but compact H₂ bow at P.A. $\approx 55^\circ$ about 1' from HW2. The current orientation of the HW2 radio jet continues this clockwise migration of outflow orientations and has P.A. $\approx 45^\circ$. The chains of H₂ knots get progressively shorter as the axes rotate clockwise toward decreasing P.A.. This remarkable progression may be an indication that HW2 powers a pulsed and precessing jet. Between each major outflow ejection event, the jet orientation changes by about 10°–15° as seen in projection on the plane of the sky.

A rough dynamical age for each chain can be estimated by dividing the length of each by the velocity of its tip. The radial velocities of the HH objects located at the ends of the first three chains are low ($v < 60$ km s⁻¹), indicating that they are most likely moving close to the plane of the sky. Fabry–Perot imaging of the H₂ emission (Hiriart et al. 2004) also indicates low, but chaotic, radial velocities. On the other hand, the excitation of the visual wavelength H α and S II emission of the eastern HH objects and comparison with the speeds of other HH objects located at similar distances from their sources, indicate that shock speeds of order 100 km s⁻¹ are not unreasonable. Future proper motion measurements are needed to

determine the velocities of the ejecta. Assuming 100 km s⁻¹ (reasonable for similar shocks exhibiting NIR H₂ emission, e.g. Reipurth & Bally 2001), the dynamical ages of the four eastern H₂ chains are 9900, 7000, 4500, and 2100 years, respectively, indicating that an eruption/ejection event occurs approximately every 2500 years. Furthermore, the presence of the HW2 radio jet indicates that there is currently an eruption underway.

This periodic, geometric progression suggests an underlying temporal sequence. We propose a model for Cep A East in which the accretion disk surrounding HW2, responsible for launching a bipolar jet along the disk rotation axis, has periodically changed its orientation. In this picture, the easternmost lobe (position angle 90°) constitutes the oldest tracer of past jet activity. Since its launch, the accretion disk and associated bipolar jet at HW2 have been periodically torqued through a series of new orientations.

Periastron passages of a companion in an eccentric orbit that is not coplanar with the disk can readily explain the torques required to explain both the impulsive nature of the HW2 outflow, and the periodic changes in disk orientation. A cluster member in an elliptical orbit around HW2, with a periastron distance of order the disk radius, will exchange angular momentum with the disk. If the binary and disk axes are not aligned, the result is a progressive tilting of the disk at each periastron passage. The close passage of the orbiting companion will also disturb the disk during periastron passage, triggering an increase in the accretion rate onto the central star, and consequent mass loss in the form of a collimated jet. The periodic reorientation of the jet axis and disk, and the episodic character of the outflow, may be the signatures of a crowded and dynamically active environment surrounding HW2.

The angular extent of the longest shock lobe (position angle 90°) is 4.8 arcmin, yielding a projected length of about 1 pc given the adopted distance of 725 pc (Blaauw et al. 1959). As estimated above, the time between disk reorientations (and in this model, the orbital period) is ≈ 2500 years. The mass of HW2 is about 15 M_\odot (Patel et al. 2005, and references therein), so a less massive companion must have an orbital semimajor axis of ≈ 400 AU. The periastron distance must be somewhat smaller than this value. As indicated in the Introduction, Cep A HW2 has at least two companions within the required distance, including the “hot core” that may be heated by a moderate-mass protostar (Martín-Pintado et al. 2005) and the source of the expanding maser ring (Torrelles et al. 2001b; Curiel et al. 2002).

3. NUMERICAL MODELING

The interaction of a binary companion and a circumstellar disk can cause the disk to precess (e.g. Papaloizou & Terquem 1995; Terquem et al. 1999). This precession may be traced by the orientation of the jet, and has been implicated in the appearance of several precessing outflows (e.g. Eisloffel et al. 1996; Davis et al. 1997). During repeated encounters of a captured companion on an eccentric orbit, the disk orientation moves through several angles impulsively (Moeckel & Bally 2006), rather than smoothly varying as would occur in a nearly circular binary. Inspired by the observations presented above, we searched the parameter space of encounters simulated in Moeckel & Bally (2007a) and selected three combinations of parameters for further investigation.

3.1. Method and initial conditions

Table 2
SIMULATION PARAMETERS.

M_{primary} M_{\odot}	M_{disk} M_{\odot}	r_{disk} AU	M_{impactor} M_{\odot}	i degrees	r_{peri} AU
15	1.5	350	5	30	150
15	1.5	350	5	45	80
15	1.5	350	5	135	80

We used a modified version of the SPH/ N -body code GADGET-2 (Springel 2005) to model interactions between a massive protostar and a captured companion. The models and the method are similar to those of Moeckel & Bally (2006), and we summarize them here. A Keplerian disk is set up with surface density $\Sigma(r) \propto r^{-1}$, and temperature $T(r) \propto r^{-1/2}$. This disk is allowed to evolve in isolation until the system has relaxed from its initial conditions. At this time an impactor star is introduced on a slightly hyperbolic orbit ~ 3 disk radii from the primary. The stars are modeled as point masses interacting with the gas only through gravity, and are assigned an accretion radius. Gas that falls into the accretion radius and is energetically bound to the star is removed from the calculation, and its momentum and mass are added to the star. The encounter is integrated until the orbital parameters of the two stars have stopped evolving.

If the orbital timescale of the newly formed binary is much larger than the orbital period of the disk, the system is analytically advanced to the next interaction. Each gas particle is either assigned to the star that it is most bound to or deemed ejected from the system, giving us three populations. The ejected material is removed from the calculation. In order to determine a Keplerian orbit, the gas that remains and the star that it is bound to are treated as a point mass at their center of mass, and these point masses are analytically advanced to the next encounter. Upon restarting the hydrodynamic simulation, the gas particles are circularized about their star using a technique described in greater detail in Moeckel & Bally (2006). The main point of this process is that we avoid a computationally expensive integration to apastron and back.

Moeckel & Bally (2007a) performed simulations of encounters between a $20 M_{\odot}$ star with a $2 M_{\odot}$, 500 AU disk and impactors of varying masses, periastron, and inclination angle. By inspecting these simulations for disk orientation changes of roughly 10° , we selected three impactor parameters to study the HW2 system, shown in Table 2. We scaled the primary and disk masses down to values perhaps more suitable for HW2, a $15 M_{\odot}$ primary with 350 AU, $1.5 M_{\odot}$ disk. The mass of the impactor in all cases is $5 M_{\odot}$; a fairly massive companion is needed to torque the disk through $\sim 10^{\circ}$ during a periastron passage. We modeled the disk using $\sim 1.28 \times 10^5$ particles, and followed each system through three encounters.

3.2. Numerical results

We consider the orientation of the inner disk \hat{L}_{disk} to be defined by the summed angular momenta of the gas particles within 30 AU of the primary. In order to determine what the outflow appearance would be, we construct a crude jet model as follows. We assume that the orientation of the outflow is the same as the inner disk orientation, $\hat{V}_{\text{jet}} \equiv \hat{L}_{\text{disk}}$. By assuming a constant-velocity jet launched in this direction, we can construct a model of what the jet from this interacting system will look like. Of the three cases considered, the two prograde simulations ($i = 30^{\circ}$ and $i = 45^{\circ}$) produced jets that are

similar in appearance to the observed system. The retrograde encounter, $i = 135^{\circ}$, showed a shift in orientation similar to the other two for the first passage, but the subsequent passages did not resemble the actual jet. We believe this is in part due to the rapid disk destruction associated with retrograde passages having small $r_{\text{peri}}/r_{\text{disk}}$ (Moeckel & Bally 2006).

Plots of the jets through the first three passages from the two prograde simulations are shown in Figure 7. They have been rotated about the initial jet axis in order to most closely match the observed appearance of the HW2 system, and the initial jet axis lies on the x-axis to match the orientation of the jet lobes in Figure 6. The simulations yield the elapsed time of the encounters, and at an assumed distance of 725 pc, the distance to the oldest bowshock is approximately 1 pc. By choosing the velocity of the jet to match this distance, we find jet velocities of 88 km s^{-1} for the 30° case, and 139 km s^{-1} for the 45° case. The boxes on the figure indicate where bowshocks would be expected, and are labeled with the age of the flow at that point. While both simulations capture the qualitative orientation of the jet, the case with $i = 45^{\circ}$ appears to match the observed jet orientation slightly better.

We stress that we are not claiming that the parameters studied here reflect the reality of the HW2 region’s dynamics. The uncertainties in the masses, radii, and even number of objects impede attempts to model the actual system, and the range of parameters that produce similar outflows is large. Rather, these simulations should be viewed as a proof-of-concept experiment. Using plausible values for the masses of the components, we can generate outflow orientations similar to those observed, via a series of postcapture interactions between a massive protostellar system and a moderate-mass companion.

4. DISCUSSION

The two most massive protostellar objects in Cep A, HW2 and HW3c, each power separate outflows. HW2 appears to have been responsible for at least four quasi-periodic ejections that produced collimated flows visible in NIR H_2 emission in the eastern lobe of the Cep A outflow complex. While the first eruption launched a flow nearly due east, subsequent ejections indicate that the source orientation rotated north by about 10° between events. The current orientation of the radio jet, rotated clockwise by 45° compared to the ejection axis of the first event, continues this trend. Radial velocity measurements of the visual wavelength emission associated with HH 169 and 174 located at the tips of three of the outflow axes indicate low radial velocities and dispersions, an indication that the outflow axis probably lies close to the plane of the sky.

The bright NIR reflection nebula emerging from the vicinity of HW2 has an axis close to the last two ejection events. Millimeter wavelength CO emission toward the eastern lobe of the Cep A outflow complex reveals two ridges of blueshifted emission at P.A. $\sim 100^{\circ}$ and 35° , approximately symmetrically placed about the axis of the reflection nebula. A pair of redshifted ridges of CO emission are located on the opposite side of HW2 toward the southwest. These CO features may define the walls of an outflow cavity created by the outflow over time. The CO outflow from HW3c is superimposed on the east–west rim of this suspected cavity.

The data presented above are interpreted in terms of a pulsed, precessing jet emerging from Cep A HW2. A numerical model is used to show that a pulsed, precessing jet can be the result of disk perturbations produced by a companion star in an eccentric orbit that is not co-planar with the disk. This scenario is the most likely outcome of the capture-formed bi-

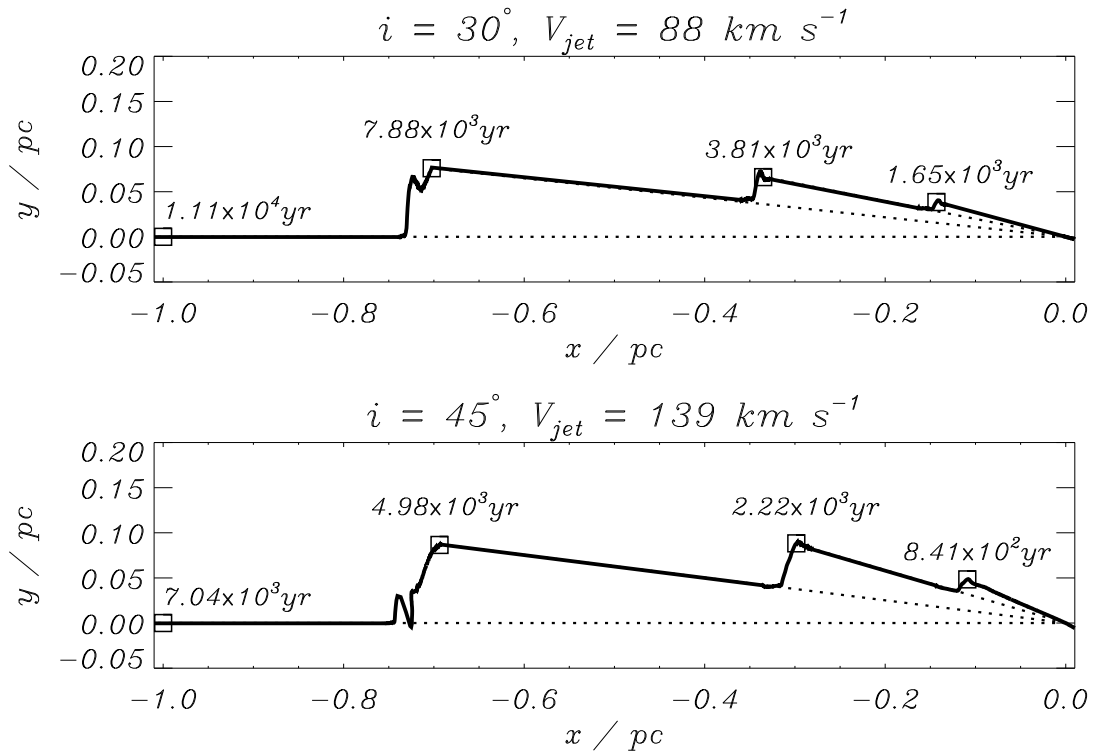


Figure 7. Locations of jet ejecta from two simulations, each as viewed at a single time. The solid lines mark projected distance from outflow source, with older material at far left and recent ejecta at far right. Dotted lines indicate successive jet orientations; in the absence of disk precession, the jet would remain horizontal. The jet velocities have been scaled to give a 1 pc distance to the oldest shock, and the initial jet orientation has been chosen for comparison to Figure 6. Boxes indicate where shocks at the ends of the outflow lobes would be expected, and are labeled with the age of the flow at that point.

nary proposed by (Moeckel & Bally 2007a,b). We note that Narayanan & Walker (1996) also suggested periodic outflow from Cep A, although the dynamical timescale they determined for the launch of successive CO shells is $\sim 1.6 \times 10^5 \text{ yr}$, two orders of magnitude greater than the $\sim 2500 \text{ yr}$ timescale suggested by the higher velocity shocked H_2 gas presented here.

The second outflow from the Cep A core region appears to emerge from slightly south of HW2. This flow is associated with a low-velocity blueshifted lobe of CO emission that terminates about 1.5 to $2'$ to the east in a faint but large H_2 bow shock. HW3d is associated with strong H_2O masers that are located at the base of a chain of radio sources at position angle P.A. $\approx 105^\circ$ (Torrelles et al. 1998, 2001a) that has the spectral index and morphology of a thermal radio jet that has the same orientation as the suspected large-scale outflow from HW3c.

A third young star located southwest of HW2 may also power an outflow that produced the radio sources HW1b, 3a, and 3b. HW3b is the third source in Cep A to contain masers (Torrelles et al. 1998, 2001a). The submillimeter source SMA4 (Brogan et al. 2007) is located on the axis of this chain close to HW3b. The chain of radio sources has a position angle P.A. $\approx 60\text{--}65^\circ$ (or 240 to 245°), close to the orientation of the H_2 jet associated with the third suspected eruption of HW2. Thus, an alternative to our model is that this collimated component east of the Cep A core is a steady jet associated with a protostar located in the HW1b, 3a, and 3b chain. If SMA4 is the source, then the chain of radio sources is the counter-jet associated with the prominent H_2 feature. However, this model does not explain the orderly progression of terminal bow-shock orientations and distances discussed above. Furthermore, the chain of radio sources HW1b, 3a,

and 3b lies in the "line-of-fire" of the current HW2 jet. Thus, it is possible to interpret these features as shocks where the HW2 jet rams part of the Cep A molecular cloud, or the outflow from HW3c.

No NIR continuum source is detected at the location of radio source W at the eastern end of HH 168. The presence of radio continuum and X-ray emission from this portion of HH 168 may indicate that this region is being impacted by shocks with speeds of at least 400 km s^{-1} . We propose that HH 168 marks the location where the HW3c outflow collides with the outflow from HW2. The location of HH 168 indicates that the currently shocked gas is mostly excited by the debris from the third and fourth eruptions of HW2 with the flow from HW3c. Ejecta from the fifth eruption, which is traced by the HW2 radio continuum jet, has not yet reached the interaction region. If HW3b also drives its own jet with an orientation similar to the third eruption from HW2, it may also contribute to the excitation of HH 168.

The complex shock morphology may be the result of turbulent mixing of the colliding flows. The north-to-south density gradient in the ambient molecular cloud may contribute to the bending of this shock complex toward the north. The CO emission, which is both red- and blueshifted at the location of HH 168, may also be deflected along our line of sight by this gradient to produce the blueshifted CO lobe farther downstream.

Collisions between outflows and clouds have been invoked to explain the complex structure of some Herbig-Haro objects such as HH 110 in Orion where the HH 270 jet slams into a small molecular cloud in the L1617 complex (López et al. 2005). An embedded IR source in this cloud, IRAS 05487+0255, drives a jet and molecular out-

flow (Reipurth & Olberg 1991; Lee et al. 2000). Kajdic et al. (2009, in preparation) propose that HH 110 is formed by the collision of the HH 270 flow with the flow from IRAS 05487+0255. Theoretical models of jet–cloud interactions were presented by Canto & Raga (1996); Raga & Canto (1996); de Gouveia Dal Pino (1999); Raga et al. (2002). Jet–jet collisions were modeled by Cunningham et al. (2006). In Cep A, HH 168 may be excited by the collision between a pair of outflows and be additionally deflected by the density gradient in the cloud. Observations show that the sources of the HW2 and 3c flows are physically close. Furthermore, both sources appear to drive flows that are close to the plane of the sky. These factors make a collision of flows reasonably probable. The absence of obvious shocks southwest of the Cep A core supports the view that ejecta from HW2 are deflected. Still, the presence of low-velocity CO emission southwest of HW2 and HW3c indicates that this part of the cloud has been impacted by outflow activity. A possible explanation for this dichotomy is that, in the distant past, only the outflow from HW2 was active, and that the deflection of this flow by the flow from HW3c is a relatively recent phenomenon.

5. CONCLUSIONS

We present new narrowband NIR images of the the Cep A outflow complex in the $2.12\ \mu\text{m}$ S(1) line of H_2 . These images provide evidence for two major outflows from the two most luminous members of the Cep A outflow complex.

The radio source HW3c appears to drive a collimated east–west outflow with a redshifted lobe emerging toward P.A. $\approx 275^\circ$ that may be responsible for much of the emission associated with HH 168 in Cep A West. The blueshifted lobe of this outflow appears to terminate in a large but faint H_2 bow shock located about $1.5\text{--}2'$ east of HW3c. The H_2 bow and the brightest portion of HH 168 are placed symmetrically about HW3c. The three H_2 bow shocks located along the southern portion of HH 168 have orientations consistent with being driven by this source.

The radio source HW2, the most luminous and massive protostar in the Cep A complex, appears to drive a precessing and pulsed jet. The H_2 images reveal four distinct jet axes. The longest and oldest outflow lobe terminates in HH 174 about $5'$ due east of HW2. The second and third lobes are progressively shorter, have rotated clockwise by about $10\text{--}15^\circ$ between ejections, and terminate in the western and eastern components of HH 169. The fourth ejection is the shortest lobe and was ejected toward the northeast, but has no visual wavelength HH objects associated with it, probably due to the high obscuration. The radio continuum jet may trace a current period of activity and continues the trend of clockwise rotation of the outflow axes. Thus, over the past 10^4 years, the HW2 outflow appears to have precessed by nearly 45° in a clockwise direction as seen on the plane of the sky. Assum-

ing an average flow speed of $100\ \text{km s}^{-1}$, HW2 undergoes an eruption about every 2500 years.

Most massive stars are born in clusters, and Cep A is no exception. In an environment with a high stellar density, interactions between a massive star and its siblings become relatively common. Cep A HW2 is surrounded by a disk at least several hundred AU in radius and with a mass of order $1\ M_\odot$. This disk can serve as a dissipative environment, and any star passing within about a disk radius has a high probability of being captured into a highly eccentric orbit. The more massive the intruder, the higher its probability of capture (Moeckel & Bally 2007a,b). This mechanism provides a natural explanation for the presence of a moderate-mass companion, indicated in the HW2 system by a hot core $0.6''$ (400 AU in projection) east of HW2 (Martín-Pintado et al. 2005).

It is proposed that Cep A HW2 has a moderate-mass companion in an eccentric orbit whose orbital plane is inclined with respect to the circumstellar disk surrounding HW2. Periastron passages of the companion may perturb the disk, and drive accretion onto the central star, and produce quasi-periodic episodes of collimated mass ejection. The non-coplanar eccentric orbit also applies a torque to the disk, changing its orientation. We investigate this hypothesis using an SPH code and demonstrate that such interactions can result in the type of disk orientation change proposed to have occurred in Cep A. Modeling indicates that a companion in a prograde orbit inclined with respect to the HW2 disk by about 40° fits the observations best. Because an impactor mass greater than the disk mass is needed to torque the disk through an appreciable angle, the presence of one or more low-mass sources in the vicinity do not affect this model.

The bright shock complex HH 168 may be excited by the collision of two or more outflows emerging from the Cep A cloud core located about $90''$ to the east. The western end of HH 168 may trace the chaotic mixing resulting from the collision of the steady (in orientation) flow from HW3c and the third eruption of HW2; the eastern end of HH 168 may trace the collision of the flow from HW3c with the fourth eruption of HW2. If SMA4 also drives a flow, it may also participate in this interaction.

This work was supported by NSF grant AST0407356 and the CU Center for Astrobiology funded by NASA under cooperative agreement no. NNA04CC11A issued by the Office of Space Science. Some of the observations presented were obtained with the Apache Point Observatory 3.5-meter telescope, which is owned and operated by the Astrophysical Research Consortium. We thank Drs. Mark Morris and Ralph Shuping for assistance with the acquisition and reduction of the Keck data.

REFERENCES

- Bally, J., Devine, D., Fesen, R. A., & Lane, A. P. 1995, *ApJ*, 454, 345
 Bally, J., & Lane, A. P. 1990, in *ASP Conf. Ser. 14: Astrophysics with Infrared Arrays*, ed. R. Elston (San Francisco: ASP), 273
 Bally, J., Licht, D., Smith, N., & Walawender, J. 2006, *AJ*, 131, 473
 Bally, J., & Reipurth, B. 2001, *ApJ*, 546, 299
 Blaauw, A., Hiltner, W. A., & Johnson, H. L. 1959, *ApJ*, 130, 69
 Brogan, C. L., Chandler, C. J., Hunter, T. R., Shirley, Y. L., & Sarma, A. P. 2007, *ApJ*, 660, L133
 Canto, J., & Raga, A. C. 1996, *MNRAS*, 280, 559
 Cohen, R. J., Rowland, P. R., & Blair, M. M. 1984, *MNRAS*, 210, 425
 Colome, C., & Harvey, P. M. 1995, *ApJ*, 449, 656
 Comito, C., Schilke, P., Endesfelder, U., Jiménez-Serra, I., & Martín-Pintado, J. 2007, *A&A*, 469, 207
 Crawford, D. L., & Barnes, J. V. 1970, *AJ*, 75, 952
 Cunningham, A. J., Frank, A., & Blackman, E. G. 2006, *ApJ*, 646, 1059
 Curiel, S., Ho, P. T. P., Patel, N. A., Torrelles, J. M., Rodríguez, L. F., Trinidad, M. A., Cantó, J., Hernández, L., Gómez, J. F., Garay, G., & Anglada, G. 2006, *ApJ*, 638, 878
 Curiel, S., Trinidad, M. A., Cantó, J., Rodríguez, L. F., Torrelles, J. M., Ho, P. T. P., Patel, N. A., Greenhill, L., Gómez, J. F., Garay, G., Hernández, L., Contreras, M. E., & Anglada, G. 2002, *ApJ*, 564, L35
 Davis, C. J., Eisloffel, J., Ray, T. P., & Jenness, T. 1997, *A&A*, 324, 1013

- de Gouveia Dal Pino, E. M. 1999, *ApJ*, 526, 862
- Devine, D., Bally, J., Reipurth, B., & Heathcote, S. 1997, *AJ*, 114, 2095
- Eisloffel, J., Smith, M. D., Davis, C. J., & Ray, T. P. 1996, *AJ*, 112, 2086
- Garay, G., Ramirez, S., Rodríguez, L. F., Curiel, S., & Torrelles, J. M. 1996, *ApJ*, 459, 193
- Goetz, J. A., Pipher, J. L., Forrest, W. J., Watson, D. M., Raines, S. N., Woodward, C. E., Greenhouse, M. A., Smith, H. A., Hughes, V. A., & Fischer, J. 1998, *ApJ*, 504, 359
- Gómez, J. F., Sargent, A. I., Torrelles, J. M., Ho, P. T. P., Rodríguez, L. F., Cantó, J., & Garay, G. 1999, *ApJ*, 514, 287
- Gutermuth, R. A., Megeath, S. T., Pipher, J. L., Allen, T. S., Williams, J. P., Allen, L. E., Myers, P. C., & Fazio, G. G. 2005, in *Protostars and Planets V* (Waikoloa, Hawaii), 8585
- Hartigan, P., Lada, C. J., Tapia, S., & Stocke, J. 1986, *AJ*, 92, 1155
- Hartigan, P., Morse, J., & Bally, J. 2000, *AJ*, 120, 1436
- Hiriart, D., Salas, L., & Cruz-González, I. 2004, *AJ*, 128, 2917
- Hoare, M. G., & Garrington, S. T. 1995, *ApJ*, 449, 874
- Hughes, V. A., Cohen, R. J., & Garrington, S. 1995, *MNRAS*, 272, 469
- Hughes, V. A., & Wouterloot, J. G. A. 1984, *ApJ*, 276, 204
- Jiménez-Serra, I., Martín-Pintado, J., Rodríguez-Franco, A., Chandler, C., Comito, C., & Schilke, P. 2007, *ApJ*, 661, L187
- Jones, B., & Puetter, R. C. 1993, *Proc. SPIE*, 1946, 610
- Koppelaar, K., van Duinen, R. J., Aalders, J. W. G., Sargent, A. I., & Nordh, L. 1979, *A&A*, 75, L1
- Lee, C.-F., Mundy, L. G., Reipurth, B., Ostriker, E. C., & Stone, J. M. 2000, *ApJ*, 542, 925
- López, R., Estalella, R., Raga, A. C., Riera, A., Reipurth, B., & Heathcote, S. R. 2005, *A&A*, 432, 567
- Martín-Pintado, J., Jiménez-Serra, I., Rodríguez-Franco, A., Martín, S., & Thum, C. 2005, *ApJ*, 628, L61
- Moeckel, N., & Bally, J. 2006, *ApJ*, 653, 437
- . 2007a, *ApJ*, 656, 275
- . 2007b, *ApJ*, 661, L183
- Narayanan, G., & Walker, C. K. 1996, *ApJ*, 466, 844
- Papaloizou, J. C. B., & Terquem, C. 1995, *MNRAS*, 274, 987
- Patel, N. A., Curiel, S., Sridharan, T. K., Zhang, Q., Hunter, T. R., Ho, P. T. P., Torrelles, J. M., Moran, J. M., Gómez, J. F., & Anglada, G. 2005, *Nature*, 437, 109
- Pravdo, S. H., & Tsuboi, Y. 2005, *ApJ*, 626, 272
- Raga, A. C., & Canto, J. 1996, *MNRAS*, 280, 567
- Raga, A. C., de Gouveia Dal Pino, E. M., Noriega-Crespo, A., Mininni, P. D., & Velázquez, P. F. 2002, *A&A*, 392, 267
- Reipurth, B., & Bally, J. 2001, *ARA&A*, 39, 403
- Reipurth, B., & Olberg, M. 1991, *A&A*, 246, 535
- Rodríguez, L. F., Garay, G., Curiel, S., Ramirez, S., Torrelles, J. M., Gomez, Y., & Velázquez, A. 1994, *ApJ*, 430, L65
- Rodríguez, L. F., Ho, P. T. P., & Moran, J. M. 1980a, *ApJ*, 240, L149
- Rodríguez, L. F., Moran, J. M., Ho, P. T. P., & Gottlieb, E. W. 1980b, *ApJ*, 235, 845
- Rodríguez, L. F., Torrelles, J. M., Raga, A. C., Cantó, J., Curiel, S., & Garay, G. 2005, *Rev. Mexicana Astron. AstroPs.*, 41, 435
- Sargent, A. I. 1977, *ApJ*, 218, 736
- . 1979, *ApJ*, 233, 163
- Shuping, R. Y., Morris, M., & Bally, J. 2004, *AJ*, 128, 363
- Springel, V. 2005, *MNRAS*, 364, 1105
- Su, Y.-N., Liu, S.-Y., Chen, H.-R., Zhang, Q., & Cesaroni, R. 2007, *ApJ*, 671, 571
- Terquem, C., Eisloffel, J., Papaloizou, J. C. B., & Nelson, R. P. 1999, *ApJ*, 512, L131
- Torrelles, J. M., Gómez, J. F., Garay, G., Rodríguez, L. F., Curiel, S., Cohen, R. J., & Ho, P. T. P. 1998, *ApJ*, 509, 262
- Torrelles, J. M., Patel, N. A., Curiel, S., Ho, P. T. P., Garay, G., & Rodríguez, L. F. 2007, *ApJ*, 666, L37
- Torrelles, J. M., Patel, N. A., Gómez, J. F., Ho, P. T. P., Rodríguez, L. F., Anglada, G., Garay, G., Greenhill, L., Curiel, S., & Cantó, J. 2001a, *ApJ*, 560, 853
- . 2001b, *Nature*, 411, 277
- Torrelles, J. M., Verdes-Montenegro, L., Ho, P. T. P., Rodríguez, L. F., & Canto, J. 1993, *ApJ*, 410, 202
- Yu, K. C., Billawala, Y., & Bally, J. 1999, *AJ*, 118, 2940